Curve- and Surface-based Registration of Lung CT images via Currents

Vladlena Gorbunova[1], Stanley Durrleman[2,3], Pechin Lo[1], Xavier Pennec[2], and Marleen de Bruijne[1,4]

[1] Department of Computer Science, University of Copenhagen, Denmark
[2] Asclepios, INRIA Sophia Antipolis, France
[3] Centre de Mathematique et Leurs Application, ENS Cachan, France
[4] Biomedical Imaging Group Rotterdam, Erasmus MC, Rotterdam, the Netherlands

Abstract. Feature-based registration methods offer a robust alternative to intensity-based methods when intensities change because of pathology, image artifacts or differences in acquisition. For registration of lung CT images, we propose to use distinctive anatomical structures, such as the pulmonary vessel tree centerlines and lung surfaces, to establish correspondences between pairs of scans. In this respect, we develop and evaluate a curve- and surface-based registration method using currents. This method does not require point correspondence between structures. We conducted experiments on five pairs of images, where each pair consists of image volumes extracted at the end inhale and end exhale phases of a 4D-CT scan. To evaluate the registration, we used a set of 300 anatomical landmarks marked on each image pair. Using both vessel centerlines curves and lung surfaces yields better alignment (median error of 1.85 mm) than using only curves (2.37 mm) or surfaces (3.53 mm). The combined method achieves overall registration accuracy comparable to that of intensity-based registration, whereas the errors are made in different locations. This suggests that low dimensional geometrical features capture sufficient information to drive a reliable registration, while results can still be improved by combining intensity and feature based registration approaches into one framework.

1   Introduction

Registration of chest CT scans is an important subject within pulmonary image analysis. The general task of registration is to establish a point-to-point correspondence between two images. Registration of lung CT images can be used in various clinical applications, such as lung cancer radiotherapy planning and quantitative analysis of disease progression.

Image registration methods can be separated into two general groups: intensity-based and feature-based methods. Intensity-based methods integrate spatial information over the entire image domain, whereas feature-based methods require a representation of the image data in terms of distinctive geometrical structures. Feature-based methods offer more robust registration when image intensity is

changed, owning to for instance pathology, image artifacts or differences in scan
protocol. Generally, segmentation of geometrical structures in lungs is less sen-
sitive to intensity changes, since the method incorporates geometrical regularity
constraints or prior anatomical knowledge. Moreover, segmentation of distinctive
lung structures may be either corrected manually or delineated by a professional.

The most distinctive anatomical structures in lung CT images are vessels,
airways, lobe fissures and lung surfaces. Lungs surface and lobe fissures define
large-scale deformations of the lungs and provide an insight into the global mo-
tion of the lungs, while small-scale deformations are influenced by vessels and
airway tree motion.

Feature-based registration relies on various geometrical structures, e.g., points,
curves or surfaces. Thin-plate spline image registration [1–3] is the standard
method for matching points under the assumption that deformations are small.
For large deformations, a diffeomorphic point matching approach was developed
by Joshi and Miller [4] and was later adapted for surface matching [5]. Current-
based diffeomorphic method for surface matching under the large deformations,
pioneered by Glaunès et. al. [5], was further developed and adapted for curve
matching problem [6, 7]. Within a framework of currents, no point correspon-
dence between structures is required.

Several surface-based registration methods were previously developed for
lung CT images [8–10]. The outer surface of the lungs together with the outer
surface of vessels were used in an algorithm similar to iterative closest point
methods in [8]. Lung surface was used to register CT lung images [10] and to con-
strain intensity-based registration with a deformation field obtained from surface
matching procedure [9]. The two main advantages of the feature-based registra-
tion of lung CT images via currents are: no point correspondence is required
and unified representation of curves and surfaces. The low dimensional geomet-
rical features, such as curves and surfaces contain much fewer points compared
to dense intensity images, thus feature-based registration can be more efficient.
Moreover, in the framework of currents, dimensionality of image features may
be reduced even more without decreasing registration accuracy [11].

In this paper we apply the current-based registration method, pioneered by
Glaunès et. al. [5] and further propagated by Durrleman [7, 12], to three feature
sets: vessel centerlines, lung surface and combined set of centerlines and surface.
We evaluated the registration methods on a set of 5 pairs of end exhalation and
end inhalation phases of 4D-CT images with ground truth landmarks.

2 Registration via Currents

2.1 Representation of curves and surfaces

In the framework of currents [5, 6, 12], geometrical shapes such as curves and
surfaces are represented with a set of vectors. A current is encoded with a finite
set of vectors attached to the specified positions. A curve $C(x)$ can be defined
with its tangent vector $\tau(x)$ at each position x. In a discrete setting, curve is

considered as a set of piece-wise linear segments where each segment is represented by its center point, tangential direction, and segment length. Similarly, a surface $S(x)$, with a given mesh, is represented with the normal direction $n(x)$, face center x and area. Both surfaces and curves are thus encoded into currents as a set of vectors. Geometrical shape in the framework of currents is defined in a weak form, as the action of the shape on a test vector field w from a space of possible vector fields W. The current of a curve $C(\omega)$ is defined by the path integral along the curve through the test vector field w,

$$C(\omega) = \int_C w(x)\tau(x)dx. \qquad (1)$$

And the current of a surface $S(\omega)$ is defined by the flux of the vector field w trough the surface,

$$S(\omega) = \int_S w(x)n(x)dx. \qquad (2)$$

The space W of test vector fields is a space of square integrable vector fields convolved with a Gaussian kernel with standard deviation σ_w [12, 6]. The norm of the current, $\mu(C)$, is defined in the dual space W^*, as the maximum action of the current among all possible test vector fields $||\mu(C)||_W = \sup_{||\omega||_W \leq 1} C(w)$.

2.2   Lung structures as currents

In this paper we used distinctive anatomical lung structures such as vessels and lung surface as features for registration. Fig. 1(a) shows an example of segmented lung structures. The lung fields and vessels are segmented with the algorithm described in [14]. A sparse triangulation of the lung surface was computed via the marching cube algorithm [15]. For each face, the corresponding normals were computed and oriented to point outwards of the surface. Fig. 1(b) shows an example of the constructed current for a lung surface.

Vessel tree was segmented as follows: lung image was thresholded with a fixed intensity value $t_v = -600HU$, then a local analysis of Hessian matrix was performed in order to remove non-tube like structures. Large vessels segmented near the hilum area were omitted from the vessel tree segmentation. For more details on vessels segmentation algorithm we refer the reader to [14]. Centerlines were extracted from the segmented vessel tree using a 3D thinning algorithm [16].

The tangential direction of a centerline was computed via local principal component analysis. For each centerline point we extracted neighboring centerline points, applied PCA to the point cloud, and assigned the first principal component to the tangential direction at the centerline. For centerlines sufficiently far from vessel bifurcation and neighboring vessel, the principal direction points to a tangential direction of the centerline. For centerlines close to the bifurcation the principal direction points between the two splitting vessel centerlines. This is consistent with the framework of currents, were the action of each vessel direction results in a joint action at the bifurcation point. The orientation for the
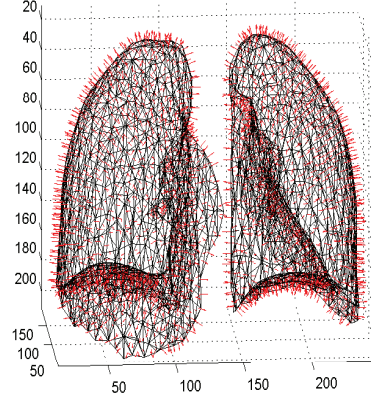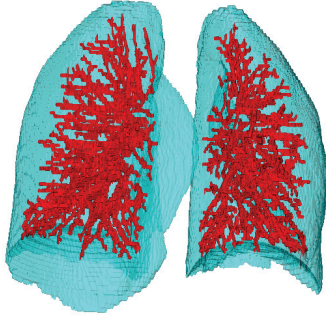
(a) Example of segmented lung surface and lung vessel tree

(b) Current corresponding to a lung surface.
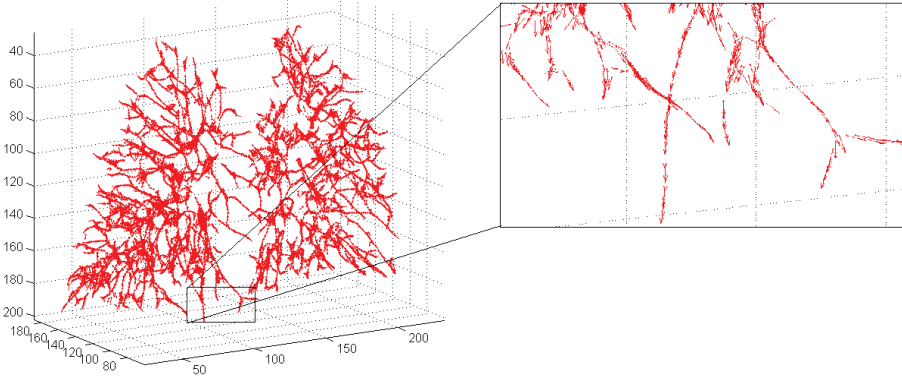
(c) Current corresponding to a vessel tree centerlines.

Fig. 1. Example of segmented lungs surface and vessel tree 1(a); triangulation of the lungs surface (black mesh) with the corresponding current (red vectors) 1(b); current corresponding to the vessel tree centerlines (red vectors) with a zoom-in 1(c).

positive direction was set to point outwards from the center of the image. Fig. 1(c) shows an example of the constructed current for a segmented vessel tree and a zoom-in into a bottom part of the image.

2.3 Current-based Image Registration

In this paper, we combine the previous work on matching curves [6] and surfaces [5] via currents. The similarity measure between two curves C_f, C_m or

two surfaces S_f, S_m is defined as the squared norm of the difference in μ for corresponding currents with respect to the test vector field $w \in W$:

$$E(C_f; C_m) = ||\mu(C_f) - \mu(\phi(C_m))||_W^2, \qquad (3)$$

for fixed and moving curves C_f and C_m respectively. And

$$E(S_f; S_m) = ||\mu(S_f) - \mu(\phi(S_m))||_W^2, \qquad (4)$$

for fixed and moving surfaces S_f and S_m respectively, where ϕ is a diffeomorphic transform function. Combining two similarity terms for curves (3), surfaces (4) and a regularisation term with trade-off coefficients $\gamma_C, \gamma_S, \gamma_\phi$ in a final cost function gives:

$$E(C_f, S_f; C_m, S_m) = \gamma_C ||\mu(C_f) - \mu(\phi(C_m))||_W^2 + \gamma_S ||\mu(S_f) - \mu(\phi(S_m))||_W^2 \\ + \gamma_\phi Reg(\phi). \qquad (5)$$

Diffeomorphic transformation ϕ of curves and surfaces was modeled in the framework of large deformation diffeomorphic matching [4,6], where deformation of each feature is defined by a velocity vector field $v_t = \phi_t'$. The smooth velocity field v_t is described via Gaussian kernel with standard deviation σ_V, where σ_V determines the typical scale of the deformations [12,6]. To guarantee smoothness of the final diffeomorphism, we defined the regularisation term as in [12],

$$Reg(\phi) = \int_0^1 ||v_t||_V^2 dt. \qquad (6)$$

3   Experiments

In order to quantify the accuracy of the proposed registration method with a ground truth, we used images from a publicly available dataset [13]. For each image pair, 300 manually placed corresponding landmarks were provided [13]. Five pairs of images, where each pair consists of images extracted at end exhale and end inhale phases of 4D CT image, were used in our experiments. In-plane resolution of the images varied from 0.97×0.97 mm to 1.16×1.16 mm and slice thickness was 2.5 mm.

3.1   Parameter Settings

Vessel tree were segmented using the algorithm as in [14] with the intensity threshold -600 HU, ratio of Hessian eigenvalues was set to $m_1 = 0.75$, $m_2 = 0.5$. For every centerline point we extracted a neighboring centerline points from the cube neighborhood of $7 \times 7 \times 7$ voxels size and computed the principal direction of the centerlines. All the direction vectors were normalized to 1. Fig. 1(c) shows an example of the extracted currents for vessel centerlines with a zoom-in to a lower part of the lungs. A regular surface triangulation was constructed with a

marching cube algorithm with further simplification of the mesh [15]. Normal directions to each of the face were normalized to 1.

In our experiments, end inhale phase of 4D-CT image was registered to end exhale phase. The following internal parameters of image registration were selected manually. The accuracy of feature alignment σ_W was set to 5 mm for curves and 10 mm for surface features. The spatial variability of deformation velocity field σ_V was set to 25 mm for both types of features. The weight coefficients in the cost function (5) were set to $\gamma_C = 1$ for the curve matching term, $\gamma_S = 0.01$ for the surface matching term and $\gamma_\phi = 10^{-4}$ for the regularizer. The cost function was minimized with a standard gradient descent approach.

3.2   Results

We evaluated four registration methods, as follows: combined curve- and surface-based registration with cost function (5); curve-based registration with cost function (3); surface-based registration with cost function (4); and a free-form B-Spline intensity-based method as in [17]. We compared registration accuracy of the four methods based on the alignment of 300 landmarks distributed uniformly in lung area, Fig. 2(b) shows an example of the spatial distribution of landmarks within the lungs.

The overall accuracy of the image registration methods was defined as the mean Euclidean distance between landmarks, target registration error (TRE), in millimeters. The mean and the standard deviation of TRE for the four methods is reported in Table 1. We performed Wilcoxon rank-sum test on TRE distribution to compare the combined curve- and surface-based registration with the curve-based and surface-based methods individually. Results are reported in the Table 1. Box-plots in Fig. 2(a) show the overall accuracy of the four image registration methods on a complete set of landmarks over all five cases.

Correlation between TRE for the intensity-based and combined curve- and surface-based registration was $\rho = 0.5$, varying from $0.17 - 0.59$ for the five cases. Overall, for 35.5% cases of landmarks the combined curve- and surface-based registration method performed better than intensity-based method.

4   Discussion

Fig. 2(a) shows that the curve-based method alone provides good registration accuracy for the majority of landmarks. However, there are many outliers present with errors of up to 2.5 cm. Within the framework of currents, points located further than the typical scale of deformations σ_V are not affected by deformations of the features, which might cause landmarks distant to the vessel centerlines to be misaligned. Surface-based registration result in a slight overall improvement in TRE compare to the initial configuration. In contrast, incorporating both surfaces and curves into feature-based registration results in more accurate registration (1.85 mm) compared to both curve-based (2.37 mm) and surface-based (3.53 mm) methods.

Table 1. Registration error at the landmark positions in [mm] for the four registration methods. The mean (m) and the standard deviation (sd) are reported. Statistical comparison of combined curve- and surface-based registration method was performed against the surface-based and curve-based methods. The notations of statistical significance level are as follows: * corresponds to $p < 0.05$ and ^{ns} to $p > 0.05$. The most right column indicates percentage of landmarks where the combined curve- and surface-based registration outperforms the intensity-based registration.

	Image Registration Accuracy in mm [m ± sd]					
N	Before	Combined	Surface	Curve	Intensity	%
1	3.89 ± 2.78	1.47 ± 0.72	$2.45 \pm 1.56^*$	$2.24 \pm 1.41^*$	1.23 ± 0.61	37.7
2	4.34 ± 3.90	2.19 ± 1.98	$3.63 \pm 2.94^*$	2.32 ± 2.06^{ns}	1.26 ± 0.67	39.0
3	6.94 ± 4.05	3.30 ± 3.05	$5.31 \pm 3.26^*$	$3.03 \pm 2.79^*$	1.86 ± 1.11	25.0
4	9.83 ± 4.86	3.34 ± 2.67	$5.98 \pm 3.74^*$	$5.28 \pm 4.52^*$	2.15 ± 1.48	36.0
5	7.48 ± 5.51	3.83 ± 3.54	$5.80 \pm 4.37^*$	$4.40 \pm 4.42^*$	2.32 ± 1.82	40.0
	All 5 cases					
	6.50 ± 4.83	2.83 ± 2.72	$4.63 \pm 3.58^*$	$3.45 \pm 3.48^*$	1.76 ± 1.31	35.5
median	5.13	1.85	3.53	2.37	1.44	

The median of TRE for the combined curve- and surface-based registration was 1.85 mm compared to 1.44 mm for the intensity-based method. Several reasons may lead to larger TRE for the combined curve- and surface-based method, such as inconsistency in segmentations of vessels in the two images. Ambiguous segmentation of lung surface near the hilum may leads to large missregistration errors in this area. Fig. 3(b) shows a difficult case in the data with irregular centerlines in the back of the lungs. Registration of lung images based on such geometrical structures as vessels centerlines and lung surfaces can be naturally improved by including airways and lung fissures into the presented framework.

In order to understand where are the main differences between the feature-based and intensity-based method, we visualized discrepancy between the two deformation fields in Fig. 3(a). For illustration purpose, we sparsely selected points where the orientation between deformation vectors were above $60°$ and with the magnitude of discrepancy vectors more than 3 mm and plotted inside the lung area. Interestingly, the discrepancy between the feature- and intensity-based methods were localized.

We further investigate image slices located at the areas where the discrepancy between the two methods was largest (blue cut planes in Fig. 3(a)). Fig. 4 shows the difference image with the moving image subtracted from the fixed image for both registration methods. Overall, lung surfaces and small vessels were aligned more accurately with the feature-based registration method.
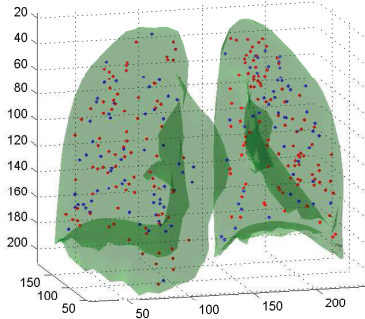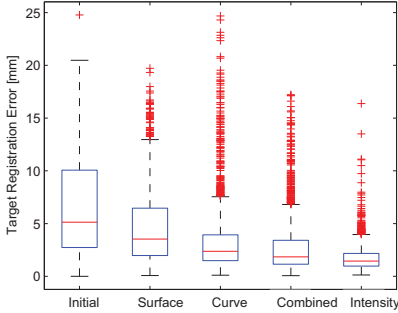
(a) Box-plot of target registration errors.

(b) Distribution of landmarks.

Fig. 2. Target registration errors (TRE) is shown in 2(a), as follows, before registration was applied (Initial), after surface-based (Suface), after curve-based (Curve), after combined curve- and surface-based (Combined) and after intensity-based registration (Intensity). Example 2(b) shows the spatial distribution of landmarks in the lungs. The landmarks, better aligned with the combined feature-based method are shown in red and with the intensity-based method in blue.

Another important component of currents is the length or the weight of the direction vector. For the task of registration of repeated lung CT images, the current for a small vessel could be given more weight than for a large vessel, leading to more accurate registration of small vessels. This is an important advantage of current-based registration over intensity-based method where small vessels with low contrast to surrounding lung tissue have negligible impact on the overall cost function. In this paper we used equal weights for all currents and normalized the length to 1.

On average, 35.5% of landmarks were aligned better with the curve- and surface-based registration. The low correlation coefficient (0.5) suggests that the two registration methods align landmarks differently and may be combined into a more robust registration method.

5   Conclusion

In this paper, a curve- and surface-based registration method is presented, where lung surface and vessel tree centerlines are built-in into the framework of current-based registration. Incorporating both centerlines and surfaces results in more accurate registration than curve- or surface-based registration method alone. The proposed combined curve- and surface-based registration method achieves slightly lower accuracy than intensity-based registration but for 35.5% of landmarks outperformed the intensity-based method. A natural extension of the
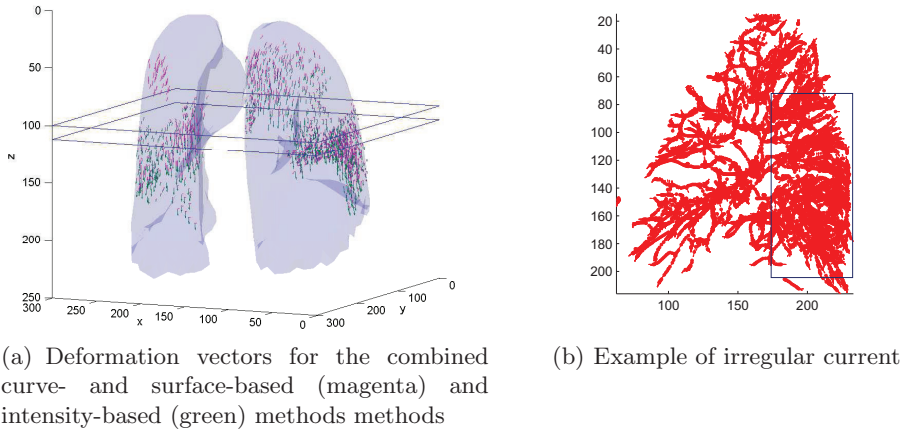
(a) Deformation vectors for the combined curve- and surface-based (magenta) and intensity-based (green) methods methods

(b) Example of irregular current

Fig. 3. (a) An example of discrepancy in deformation fields between the feature-based and intensity-based registration methods. (b) An example of an ambigious current for the back of the lung.

presented work will be incorporating more anatomical lung structures, such as airways and fissures, to improve the feature-based method.

Results show that the proposed feature-based registration method is robust to inconsistent segmentation and outliers in segmented features and capable of handling imperfect segmentations. In applications where importance of different features varies, the prior weight of a feature may be encoded into the presented registration framework. Results suggest that a natural improvement of registration would be obtained by combining the feature- and intensity-based methods.

References

1. Rohr, K., Stiehl, H.S., Sprengel, R., Buzug, T.M., Weese, J., Kuhn, M.H.: Landmark-based elastic registration using approximating thin-plate splines. IEEE Transactions on Medical Imaging **20**(6) (2001) 526–534
2. Johnson, H.J., Christensen, G.E.: Consistent landmark and intensity-based image registration. IEEE Transactions on Medical Imaging **21** (2002) 450–461
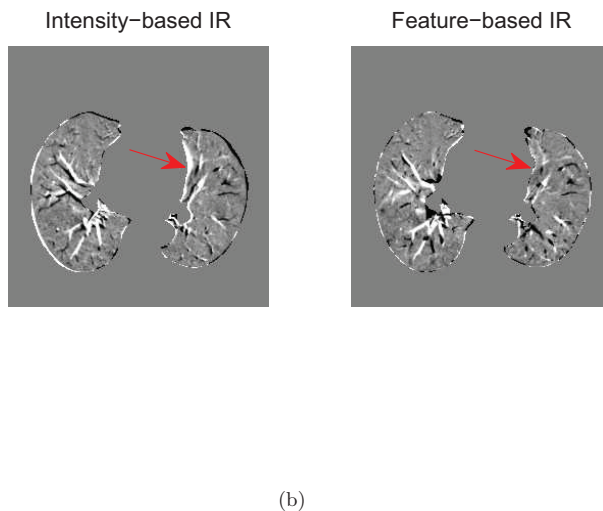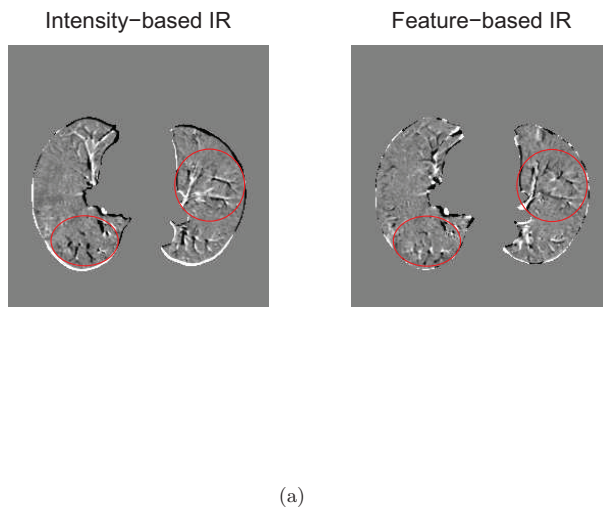
(a)

(b)

Fig. 4. Visual comparison of the combined feature-based and intensity-based registration methods. Slice cuts (a), (b) from the difference image between fixed and deformed image for the intensity- and combined feature-based registration methods were extracted on the same level as the plane cuts in Fig. 3(a). In general, the currents-based registration aligns the vessels and lung surface better, as can be seen in the areas indicated with the red circles and arrows.

3. Bookstein, F.L.: Morphological tools for landmark data; geometry and biology. Cambridge University press (1991)

4. Joshi, S.C., Miller, M.I.: Landmark matching via large deformation diffeomorphisms. IEEE Transactions on Image Processing **9** (2000) 1357–1370

5. Vaillant, M., Glaunes, J.: Surface matching via currents. Information Processing in Medical Imaging, 19th International Conference **3565** (2005) 381–392

6. Glaunès, J., Qiu, A., Miller, M.I., Younes, L.: Large deformation diffeomorphic metric curve mapping. Int. J. Comput. Vision **80**(3) (2008) 317–336

7. Durrleman, S., Pennec, X., Trouvé, A., Ayache, N.: Measuring brain variability via sulcal lines registration: a diffeomorphic approach. In: Proc. Medical Image Computing and Computer Assisted Intervention (MICCAI), Part II. Volume 4791 of LNCS. (2007) 675–682

8. Vik, T., Kabus, S., von Berg, J., Ens, K., Dries, S., Klinder, T., Lorenz, C.: Validation and comparison of registration methods for free-breathing 4D lung-CT. In: SPIE Medical Imaging. (2008)

9. Li, P., Malsch, U., Bendl, R.: Combination of intensity-based image registration with 3D simulation in radiation therapy. Phys. Med. Biol **53** (2008) 4621–4637

10. Betke, M., Hong, H., Thomas, D., Prince, C., Ko, J.P.: Landmark detection in the chest and registration of lung surfaces with an application to nodule registration. Medical Image Analysis **7**(3) (2003) 265–281

11. Durrleman, S., Pennec, X., Trouvé, A., Ayache, N.: Sparse approximation of currents for statistics on curves and surfaces. In: Proc. Medical Image Computing and Computer Assisted Intervention (MICCAI), Part II. Volume 5242 of LNCS. (2008) 390–398

12. Durrleman, S., Pennec, X., Trouvé, A., Thompson, P., Ayache, N.: Inferring brain variability from diffeomorphic deformations of currents: an integrative approach. Medical Image Analysis **12**(5) (2008) 626–637 PMID: 18658005.

13. Castillo, R., Castillo, E., Guerra, R., Johnson, V.E., McPhail, T., Garg, A.K., Guerrero, T.: A framework for evaluation of deformable image registration spatial accuracy using large landmark point sets. Physics in Medicine and Biology **54**(7) (2009) 1849–1870

14. Lo, P., Sporring, J., Ashraf, H., Pedersen, J., de Bruijne, M.: Vessel-guided airway segmentation based on voxel classification. In: Pulmonary Workshop at Medical Image Computing and Computer Assisted Intervention (MICCAI). (2008)

15. iso2mesh: A Matlab/Octave-based mesh generator. http://iso2mesh.sf.net

16. Wang, T., Basu, A.: A note on a fully parallel 3D thinning algorithm and its applications. Pattern Recognition Letters **28(4)** (2007) 501–506

17. Gorbunova, V., Lo, P., Ashraf, H., Dirksen, A., Nielsen, M., de Bruijne, M.: Weight preserving image registration for monitoring disease progression in lung CT. In: Proc. Medical Image Computing and Computer Assisted Intervention (MICCAI), Part II. Volume 5242 of LNCS. (2008) 863–870